Science
AAAS

Silica-on-Silicon Waveguide Quantum Circuits
Alberto Politi, *et al.*
Science **320**, 646 (2008);
DOI: 10.1126/science.1155441

This copy is for your personal, non-commercial use only.

If you wish to distribute this article to others, you can order high-quality copies for your colleagues, clients, or customers by clicking here.

Permission to republish or repurpose articles or portions of articles can be obtained by following the guidelines here.

The following resources related to this article are available online at www.sciencemag.org (this information is current as of September 25, 2010):

Updated information and services, including high-resolution figures, can be found in the online version of this article at:
http://www.sciencemag.org/cgi/content/full/320/5876/646

Supporting Online Material can be found at:
http://www.sciencemag.org/cgi/content/full/1155441/DC1

This article **cites 27 articles**, 3 of which can be accessed for free:
http://www.sciencemag.org/cgi/content/full/320/5876/646#otherarticles

This article has been **cited by** 66 article(s) on the ISI Web of Science.

This article has been **cited by** 3 articles hosted by HighWire Press; see:
http://www.sciencemag.org/cgi/content/full/320/5876/646#otherarticles

This article appears in the following **subject collections**:
Physics
http://www.sciencemag.org/cgi/collection/physics

Downloaded from www.sciencemag.org on September 25, 2010

Science (print ISSN 0036-8075; online ISSN 1095-9203) is published weekly, except the last week in December, by the American Association for the Advancement of Science, 1200 New York Avenue NW, Washington, DC 20005. Copyright 2008 by the American Association for the Advancement of Science; all rights reserved. The title *Science* is a registered trademark of AAAS.

then the single-pass gain must also be large in order to lase, leading to a visible nonuniformity of the lasing mode, with growth in the direction of the loss boundary (on average the radial direction for the DRL). Because the DRL has fractional finesse (which is not achievable in a 1D geometry), this effect is much larger in these systems and should be observable. This effect means that the electric field fluctuations in DRLs will differ substantially from the random matrix/quantum chaos fluctuations of linear cavity modes (*20*), first because each mode is a superposition of pseudo-random CF states and second because these CF states themselves are not uniform on average.

The coexistence of gain, nonlinear interactions, and overlapping resonances (fractional finesse) makes the DRL a more complex and richer system than the widely studied linear wave-chaotic systems. It remains to be seen whether concepts from random matrix theory and semiclassical quantum mechanics (quantum chaos) will prove fruitful in this context. The theory presented here is ab initio in the sense that it generates all properties of the lasing states from knowledge of the dielectric function of the host medium and basic parameters of the gain medium; it should be applicable to any novel laser-cavity system.

References and Notes

1. K. J. Vahala, *Nature* **424**, 839 (2003).
2. H. Cao, *J. Phys. A* **38**, 10497 (2005).
3. O. Painter *et al.*, *Science* **284**, 1819 (1999).
4. N. M. Lawandy, R. M. Balachandran, A. S. L. Gomes, E. Sauvain, *Nature* **368**, 436 (1994).
5. S. Mujumdar, M. Ricci, R. Torre, D. S. Wiersma, *Phys. Rev. Lett.* **93**, 053903 (2004).
6. H. Cao *et al.*, *Phys. Rev. Lett.* **82**, 2278 (1999).
7. H. Cao, *Waves Random Media* **13**, R1 (2003).
8. K. L. van der Molen, R. W. Tjerkstra, A. P. Mosk, A. Lagendijk, *Phys. Rev. Lett.* **98**, 143901 (2007).
9. P. Pradhan, N. Kumar, *Phys. Rev. B* **50**, 9644 (1994).
10. V. Milner, A. Z. Genack, *Phys. Rev. Lett.* **94**, 073901 (2005).
11. H. Cao, Y. Ling, J. Y. Xu, C. Q. Cao, P. Kumar, *Phys. Rev. Lett.* **86**, 4524 (2001).
12. C. Vanneste, P. Sebbah, H. Cao, *Phys. Rev. Lett.* **98**, 143902 (2007).
13. H. E. Türeci, A. D. Stone, B. Collier, *Phys. Rev. A* **74**, 043822 (2006).
14. H. E. Türeci, A. D. Stone, L. Ge, *Phys. Rev. A* **76**, 013813 (2007).
15. H. Haken, H. Sauermann, *Z. Phys.* **173**, 261 (1963).
16. H. Haken, *Light: Laser Dynamics* (North-Holland, Amsterdam, 1985), vol. 2.
17. In a high-finesse cavity, QB and CF states are essentially the same, each lasing mode is associated with one QB state, and the lasing frequency takes the value $k_\mu^{(0)}$ between the atomic line center and the cavity frequency q_1 determined by the ratio of $\gamma_\perp/\kappa$ (*13*).
18. Materials and methods are available on *Science* Online.
19. H. Kogelnik, C. V. Shank, *J. Appl. Phys.* **43**, 2327 (1972).
20. A. Kudrolli, S. Sridhar, A. Pandey, R. Ramaswamy, *Phys. Rev. E* **49**, R11 (1994).

21. This work was supported by NSF grant DMR-0408636, by the Max Kade and W. M. Keck foundations, and by the Aspen Center for Physics. We thank R. Tandy, M. Machida, H. Cao, A. Lagendijk, P. Sebbah, C. Vanneste, and D. Wiersma for discussions.

Supporting Online Material

www.sciencemag.org/cgi/content/full/320/5876/643/DC1
Materials and Methods
Figs. S1 to S3
References and Notes

16 January 2008; accepted 25 March 2008
10.1126/science.1155311

Silica-on-Silicon Waveguide Quantum Circuits

Alberto Politi, Martin J. Cryan, John G. Rarity, Siyuan Yu, Jeremy L. O'Brien*

Quantum technologies based on photons will likely require an integrated optics architecture for improved performance, miniaturization, and scalability. We demonstrate high-fidelity silica-on-silicon integrated optical realizations of key quantum photonic circuits, including two-photon quantum interference with a visibility of 94.8 ± 0.5%; a controlled-NOT gate with an average logical basis fidelity of 94.3 ± 0.2%; and a path-entangled state of two photons with fidelity of >92%. These results show that it is possible to directly "write" sophisticated photonic quantum circuits onto a silicon chip, which will be of benefit to future quantum technologies based on photons, including information processing, communication, metrology, and lithography, as well as the fundamental science of quantum optics.

Quantum information science (*1*) has shown that quantum mechanical effects can dramatically improve performance for certain tasks in communication, computation, and measurement. Of the various physical systems being pursued, single particles of light (photons) have been widely used in quantum communication (*2*), quantum metrology (*3*–*5*), and quantum lithography (*6*) settings. Low noise (or decoherence) also makes photons attractive quantum bits (or qubits), and they have emerged as a leading approach to quantum information processing (*7*).

In addition to single-photon sources (*8*) and detectors (*9*), photonic quantum technologies require sophisticated optical circuits involving high-visibility classical and quantum interference. Although a number of photonic quantum circuits have been realized for quantum metrology (*3*, *4*, *10*–*13*), lithography (*6*), quantum logic gates (*14*–*20*), and other entangling circuits (*21*–*23*), these demonstrations have relied on large-scale (bulk) optical elements bolted to large optical tables, thereby making them inherently unscalable.

We demonstrate photonic quantum circuits using silica waveguides on a silicon chip. The monolithic nature of these devices means that the correct phase can be stably realized in what would otherwise be an unstable interferometer, greatly simplifying the task of implementing sophisticated photonic quantum circuits. We fabricated hundreds of devices on a single wafer and find that performance across the devices is robust, repeatable, and well understood.

A typical photonic quantum circuit takes several optical paths or modes (some with photons, some without) and mixes them together in a linear optical network, which in general consists of nested classical and quantum interferometers (e.g., Fig. 1C). In a standard optical implementation, the photons propagate in air, and the circuit is constructed from mirrors and beam splitters (BSs), or half-reflective mirrors, which split and recombine optical modes, giving rise to both classical and quantum interference. High-visibility quantum interference (*24*) demands excellent optical mode overlap at a BS, which requires exact alignment of the modes, whereas high visibility classical interference also requires subwavelength stability of optical path lengths, which often necessitates the design and implementation of sophisticated stable interferometers. Combined with photon loss, interference visibility is the major contributor to optical quantum circuit performance.

In conventional (or classical) integrated optics devices, light is guided in waveguides—consisting of a core and slightly lower refractive index cladding (analogous to an optical fiber)—which are usually fabricated on a semiconductor chip. By careful choice of core and cladding dimensions and refractive index difference, it is possible to design such waveguides to support only a single transverse mode for a given wavelength range. Coupling between waveguides, to realize BS-like operation, can be achieved when two waveguides are brought sufficiently close together that the evanescent fields overlap; this is known as a directional coupler. By lithographically tuning the separation between the waveguides and the length of the coupler, the amount of light coupling from one waveguide into the other (the coupling ratio $1 - \eta$, where η is equivalent to BS reflectivity) can be tuned.

The most promising approach to photonic quantum circuits for practical technologies appears to be realizing integrated optics devices that operate at the single-photon level. Key require-

Centre for Quantum Photonics, H. H. Wills Physics Laboratory and Department of Electrical and Electronic Engineering, University of Bristol, Merchant Venturers Building, Woodland Road, Bristol BS8 1UB, UK.

*To whom correspondence should be addressed. E-mail: Jeremy.OBrien@bristol.ac.uk

Downloaded from www.sciencemag.org on September 25, 2010

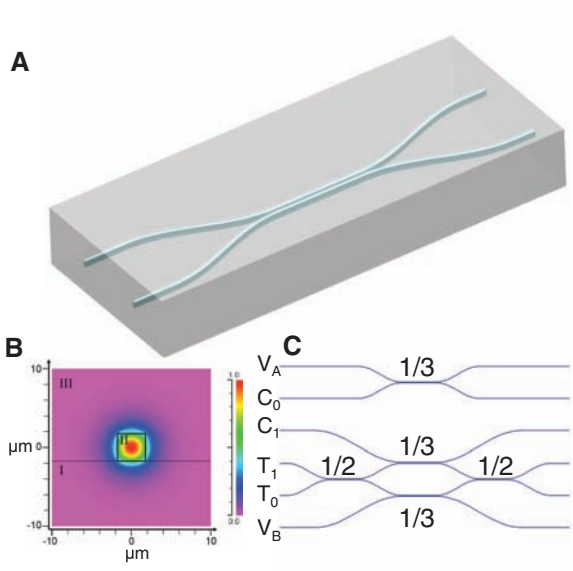

Fig. 1. Silica-on-silicon integrated quantum photonic circuits. (**A**) A directional coupler, which can be used as the building block for integrated photonic quantum circuits by replacing the bulk BS. (**B**) The modeled transverse intensity profile of the guided mode superimposed on the waveguide structure. (**C**) Design of the integrated two-photon CNOT quantum logic gate.

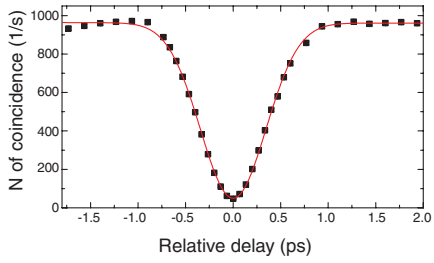

Fig. 2. Quantum interference in an integrated waveguide coupler. The plot shows the rate of detecting a photon at each output of the coupler as a function of the relative delay in arrival time of the photons. The error bars are smaller than the data points.

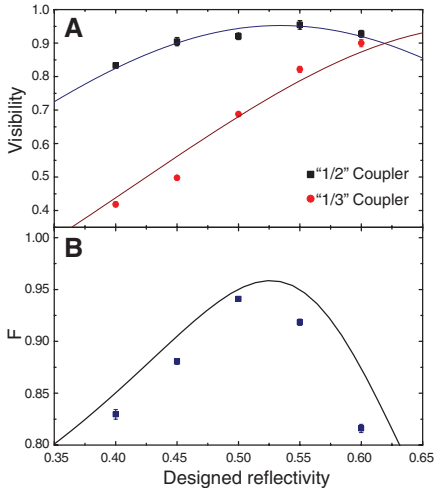

Fig. 3. Two-photon quantum interference on-chip. (**A**) Quantum interference visibility at 1/2 and 1/3 couplers that compose a CNOT gate (where the 1/2 couplers range from η (1/2) = 0.4 to 0.6 and the 1/3 couplers are 2/3 this value: η (1/3) = 0.27 to 0.4). The fit to the 1/2 data includes an offset in the coupling ratio δη and mode mismatch ε as free parameters. The same values are used for the 1/3 theoretical curve. (**B**) The average of the logical basis fidelities *F* for each of the CNOT gates. The solid curve corresponds to a model including only the above values of ε and δη. The model does not include the effect of classical interference, which explains the offset.

ments are single-mode guiding of single photons, high-visibility classical interference, high-visibility quantum interference, and the ability to combine these effects in a waveguide optical network.

We required a material system that (i) is low loss at a wavelength of λ ~ 800 nm, where commercial silicon avalanche photodiode single-photon counting modules (SPCMs) are near their peak efficiency of ~70%; (ii) enables a refractive index contrast $\Delta = (n_{core}^2 - n_{cladding}^2)/2n_{core}^2$ that results in single-mode operation for waveguide dimensions comparable to the core size of conventional single-mode optical fibers at ~ 800 nm (4 to 5 μm), to allow good coupling of photons to fiber-coupled single-photon sources and detectors; and (iii) is amenable to standard optical lithography fabrication techniques. The most promising material system to meet these requirements was silica (silicon dioxide SiO_2), with a low level of doping to control the refractive index, grown on a silicon substrate (Fig. 1B).

A refractive index contrast of Δ = 0.5% was chosen to give single-mode operation at 804 nm for 3.5 by 3.5 μm waveguides (*25*). This value of Δ provides moderate mode confinement (the transverse intensity profile is shown in Fig. 1B), thereby minimizing the effects of fabrication or modeling imperfections. We designed a number of devices, including directional couplers with various η's, Mach-Zender interferometers (consisting of two directional couplers), and more sophisticated devices built up from several directional couplers with different η's.

Starting with a 4″ silicon wafer, a 16-μm layer of thermally grown undoped silica was deposited as a buffer (material I in Fig. 1B), followed by flame hydrolysis deposition of a 3.5-μm waveguide core of silica doped with germanium and boron oxides (II). The core material was patterned into 3.5-μm-wide waveguides with standard optical lithography techniques and finally overgrown with a further 16-μm cladding layer of phosphorus and boron-doped silica with a refractive index matched to that of the buffer (III). The wafer was diced into several dozen individual chips, each containing typically several devices. Some chips were polished to enhance coupling in and out of the waveguides (*26*).

We used a beta-barium borate type-I spontaneous parametric down-conversion (SPDC) crystal, pumped with a 60-mW, 402-nm continuous wave diode laser to produce 804-nm degenerate photon pairs at a detected rate of 4000 s^{-1} when collected into single-mode polarization maintaining fibers (PMFs). We used 2-nm interference filters to ensure good spectral indistinguishability (*27*). Single photons were launched into the waveguides on the integrated optical chips and then collected at the outputs using two arrays of 8 PMFs, with 250 μm spacing, to match that of the waveguides, and detected with fiber-coupled SPCMs. The PMF arrays and chip were directly butt-coupled, with index matching fluid. Overall coupling efficiencies of ~60% through the device (insertion loss = 40%) were routinely achieved (*28*).

Figure 2 shows the classic signature of quantum interference: a dip in the rate of detecting two photons at each output of a directional coupler near zero delay in relative photon arrival time (*24*). The raw visibility (*29*) $V = 94.8 \pm 0.5\%$ is a measure of the quality of the interference and demonstrates very good quantum behavior of photons in an integrated optics architecture.

Figure 3A shows the measured nonclassical visibility for 10 couplers on a single chip with a range of design η's. The observed behavior is well explained by the theoretical curves, which include a small amount of mode mismatch ε and an offset of $\delta\eta = 3.4 \pm 0.7\%$ from the design ratio. It is inherently difficult to identify in which degree of freedom this small mode mismatch occurs (*30*). Misalignment of PMF fibers in the array (specified to be <3°) would cause polarization mode mismatch. Small spatial mode mismatch could arise if weakly guided higher-order modes propagate across the relatively short devices (*31*). These results demonstrate the high yield and excellent reproducibility of the devices.

General photonic quantum circuits require both quantum and classical interference and their combination for conditional phase shifts (*32*). An ideal device for testing all of these requirements is the entangling controlled-NOT (CNOT) logic gate shown in Fig. 1C (*33*, *34*), which has previously been experimentally demonstrated using bulk optics (*15*–*19*). The control *C* and target *T* qubits are each encoded by a photon in two waveguides, and the success of the gate is heralded by detection of a photon in both the control and target outputs, which happens with proba-

Downloaded from www.sciencemag.org on September 25, 2010

bility 1/9. The waveguide implementation of this gate is essentially a direct writing onto the chip of the theoretical scheme presented in (*33*); it is composed of two 1/2 couplers and three 1/3 couplers.

To allow for possible design and fabrication imperfections, we designed and fabricated on the same chip several CNOT devices with 1/2 couplers ranging from η (1/2) = 0.4 to 0.6 and, correspondingly, 1/3 couplers ranging from η (1/3) = 0.27 to 0.4 (i.e., 2/3 of the 1/2 couplers). The quantum interference measurements described above (Fig. 3B) show that the devices are in fact very close to the design η: δη = 3.4 ± 0.7%. To measure the 1/2 couplers, we sent single photons into the T_0 and T_1 inputs and collected photons from the C_1 and V_B outputs (and the reverse for the other 1/2 coupler); the 1/3 data are for the couplers between the C_0 and V_A waveguides (see Fig. 1C).

For the CNOT device with nominally η (1/2) = 0.5 and η (1/3) = 0.33 couplers, we input the four computational basis states $|0\rangle_C|0\rangle_T$, $|0\rangle_C|1\rangle_T$, $|1\rangle_C|0\rangle_T$, and $|1\rangle_C|1\rangle_T$ and measured the probability of detecting each of the computational basis states at the output (Fig. 4A). The excellent agreement for the $|0\rangle_C$ inputs (peak values of 98.5%) is a measure of the classical interference in the target interferometer and demonstrates that the waveguides are stable on a subwavelength scale—a key advantage arising from the monolithic nature of an integrated optics architecture. The average of the logical basis fidelities (*14*–*20*) is $F = 94.3 \pm 0.2\%$. The fidelities for the other four devices (with different η's) are lower (Fig. 3B), as expected.

To directly confirm coherent quantum operation and entanglement in our devices, we launched pairs of photons into the T_0 and T_1 waveguides. This state should ideally be transformed at the first 50:50 coupler as follows:

$$|11\rangle_{T_0T_1} \rightarrow (|20\rangle_{T_0T_1} - |02\rangle_{T_0T_1})/\sqrt{2} \quad (1)$$

that is, a maximally path-entangled superposition of two photons in the top waveguide and two photons in the bottom waveguide. A very low rate of detecting a pair of photons at the C_1 and V_A outputs, combined with a high rate of detecting two photons in either of these outputs (with a pair of cascaded SPCMs) confirmed that the state was predominantly composed of $|20\rangle$ and $|02\rangle$ components but did not indicate a coherent superposition. At the second 50:50 coupler between the T_0 and T_1 waveguides, the reverse transformation of Eq. 1 should occur, provided the minus superposition exists. A high rate of detecting photon pairs at the T_0 and T_1 outputs, combined with a low rate of detecting two photons in either of these outputs, confirmed this transformation. From each of these measured count rates, we were able to estimate the two-photon density matrix (Fig. 4D). The fidelity with the maximally path-entangled state $|20\rangle - |02\rangle$ is >92% (*35*). This high-fidelity generation of the lowest-order maximally path-entangled state, combined with confirmation of the phase stability of the superposition, demonstrates the applicability of integrated devices for quantum metrology applications.

Finally, we tested the simple quantum circuits shown in Fig. 4, B and C, consisting of a CNOT gate and Hadarmard H gates—$|0\rangle \rightarrow |0\rangle + |1\rangle$; $|1\rangle \rightarrow |0\rangle - |1\rangle$—each implemented with a 50:50 coupler between the C_0 and C_1 waveguides (*25*). In both cases, we observe good agreement with the ideal operation, as quantified by the average classical fidelity between probability distributions (*36*, *37*): 97.9 ± 0.4% and 91.5 ± 0.2%, respectively. The device shown in Fig. 4B should produce equal superpositions of the four computation basis states $|00\rangle \pm |01\rangle \pm |10\rangle \pm |11\rangle$ and that shown in Fig. 4C should produce the four maximally entangled Bell states $\Psi^{\pm} \equiv |01\rangle \pm |10\rangle$ and $\Phi^{\pm} \equiv |00\rangle \pm |11\rangle$. Although this cannot be confirmed directly on-chip, the above demonstrations of excellent logical basis operation of the CNOT and coherent quantum operation give us great confidence.

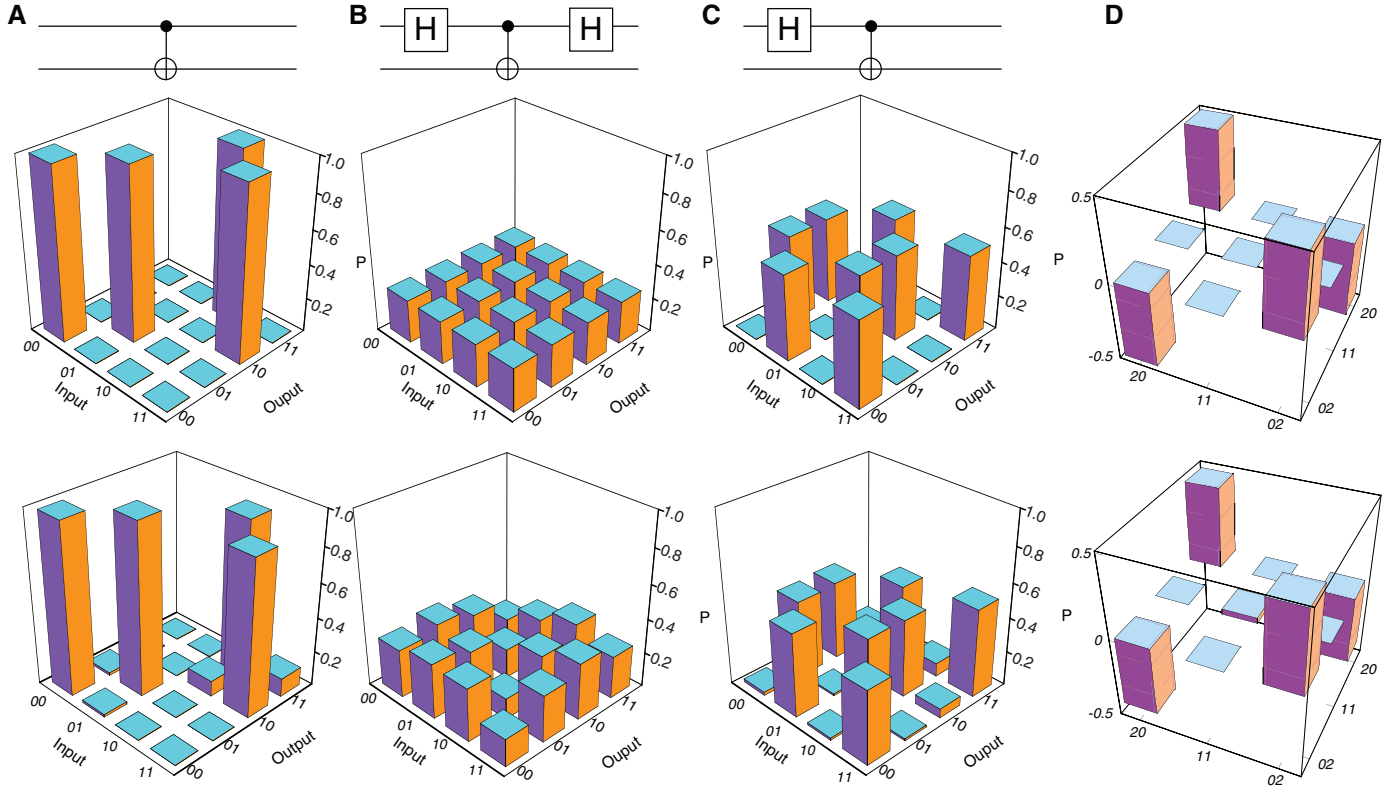

Fig. 4. Characterization of integrated quantum photonic circuits. Ideal and measured truth tables for a CNOT circuit (**A**); a CNOT with two additional H gates (**B**); and a CNOT with one additional H gate (**C**). The physical implementation fabricated on the chip is shown in fig. S1. (**D**) The ideal and estimated density matrix for the maximally path-entangled state $(|20\rangle - |02\rangle)/\sqrt{2}$.

Downloaded from www.sciencemag.org on September 25, 2010

Previous bulk optical implementations of similar photonic quantum circuits have required the design and implementation of sophisticated interferometers. Constructing such interferometers has been a major obstacle to the realization of photonic quantum circuits. The results presented here show that this problem can be drastically reduced by using waveguide devices: It becomes possible to directly write the theoretical "blackboard sketch" onto the chip, without requiring sophisticated interferometers.

We have demonstrated high-fidelity integrated implementations of each of the key components of photonic quantum circuits, as well as several small-scale circuits. This opens the way for miniaturizing, scaling, and improving the performance of photonic quantum circuits for both future quantum technologies and the next generation of fundamental quantum optics studies in the laboratory.

References and Notes

1. M. A. Nielsen, I. L. Chuang, *Quantum Computation and Quantum Information* (Cambridge University Press, 2000).
2. N. Gisin, G. Ribordy, W. Tittel, H. Zbinden, *Rev. Mod. Phys.* **74**, 145 (2002).
3. T. Nagata, R. Okamoto, J. L. O'Brien, K. Sasaki, S. Takeuchi, *Science* **316**, 726 (2007).
4. B. L. Higgins, D. W. Berry, S. D. Bartlett, H. M. Wiseman, G. J. Pryde, *Nature* **450**, 393 (2007).
5. J. L. O'Brien, *Science* **318**, 1393 (2007).
6. Y. Kawabe, H. Fujiwara, R. Okamoto, K. Sasaki, S. Takeuchi, *Opt. Express* **15**, 14244 (2007).
7. J. L. O'Brien, *Science* **318**, 1567 (2007).
8. P. Grangier, B. Sanders, J. Vuckovic, Eds., Special Issue: Focus on Single Photons on Demand, *New J. Phys.* **6** (2004).
9. A. Migdal, J. Dowling, Eds. Special Issue: Single-Photon: Detectors, Applications, and Measurement Methods, *J. Mod. Opt.* **51** (2004).
10. M. W. Mitchell, J. S. Lundeen, A. M. Steinberg, *Nature* **429**, 161 (2004).
11. P. Walther *et al.*, *Nature* **429**, 158 (2004).
12. K. J. Resch *et al.*, *Phys. Rev. Lett.* **98**, 223601 (2007).
13. F. W. Sun, B. H. Liu, Y. F. Huang, Z. Y. Ou, G. C. Guo, *Phys. Rev. A* **74**, 033812 (2006).
14. T. B. Pittman, M. J. Fitch, B. C. Jacobs, J. D. Franson, *Phys. Rev. A* **68**, 032316 (2003).
15. J. L. O'Brien, G. J. Pryde, A. G. White, T. C. Ralph, D. Branning, *Nature* **426**, 264 (2003).
16. J. L. O'Brien *et al.*, *Phys. Rev. Lett.* **93**, 080502 (2004).
17. N. K. Langford *et al.*, *Phys. Rev. Lett.* **95**, 210504 (2005).
18. N. Kiesel, C. Schmid, U. Weber, R. Ursin, H. Weinfurter, *Phys. Rev. Lett.* **95**, 210505 (2005).
19. R. Okamoto, H. F. Hofmann, S. Takeuchi, K. Sasaki, *Phys. Rev. Lett.* **95**, 210506 (2005).
20. S. Gasparoni, J.-W. Pan, P. Walther, T. Rudolph, A. Zeilinger, *Phys. Rev. Lett.* **93**, 020504 (2004).
21. P. Walther *et al.*, *Nature* **434**, 169 (2005).
22. N. Kiesel *et al.*, *Phys. Rev. Lett.* **95**, 210502 (2005).
23. C.-Y. Lu *et al.*, *Nat. Phys.* **3**, 91 (2007).
24. C. K. Hong, Z. Y. Ou, L. Mandel, *Phys. Rev. Lett.* **59**, 2044 (1987).
25. Materials and methods are available as supporting material on *Science* Online.
26. All devices were fabricated at the Centre for Integrated Photonics, CIP Technologies, www.ciphotonics.com.
27. In a separate experiment with a bulk optics BS, we used this source to observe quantum interference with $V = 97\%$.
28. Minimal effort was made to match the waveguide and fiber modes—no tapers were used, for example—and the coupling efficiency was likely limited by a mismatch of mode size and shape.
29. $V \equiv (max - min)/max$.
30. P. P. Rohde, G. J. Pryde, J. L. O'Brien, T. C. Ralph, *Phys. Rev. A* **72**, 032306 (2005).
31. The waveguides are designed such that the cut-off wavelength for higher-order modes is very near to the design wavelength in order to maintain a large waveguide core size.
32. E. Knill, R. Laflamme, G. J. Milburn, *Nature* **409**, 46 (2001).
33. T. C. Ralph, N. K. Langford, T. B. Bell, A. G. White, *Phys. Rev. A* **65**, 062324 (2002).
34. H. F. Hofmann, S. Takeuchi, *Phys. Rev. A* **66**, 024308 (2002).
35. We cannot measure the four "zero" coherences in the density matrix (although they are limited by the small $|11\rangle\langle 11|$ population) or distinguish between non-maximal coherences and rotated coherences with imaginary components for the $|20\rangle\langle 02|$ and $|02\rangle\langle 20|$ terms. However, neither of these effects changes the state fidelity. We have assumed a worst-case scenario throughout, i.e., we assume that the $|11\rangle$ component inside the interferometer makes no contribution to two-photon detection in T_0 or T_1.
36. G. J. Pryde, J. L. O'Brien, A. G. White, S. D. Bartlett, T. C. Ralph, *Phys. Rev. Lett.* **92**, 190402 (2004).
37. T. C. Ralph, S. D. Bartlett, J. L. O'Brien, G. J. Pryde, H. M. Wiseman, *Phys. Rev. A* **73**, 012113 (2006).

38. We thank A. Clark, J. Fulconis, A. Gilchrist, A. Laing, S. Lardenois, G. Maxwell, and A. Stefanov for helpful discussions. This work was supported by the U.S. Disruptive Technologies Office (DTO), the U.K. Engineering and Physical Sciences Research Council (EPSRC), the U.K. Quantum Information Processing Interdisciplinary Collaboration (QIP IRC), and the Leverhulme Trust.

Supporting Online Material

www.sciencemag.org/cgi/content/full/1155441/DC1
Materials and Methods
Fig. S1
References

21 January 2008; accepted 3 March 2008
Published online 27 March 2008;
10.1126/science.1155441
Include this information when citing this paper.

Practical Synthesis of Prostratin, DPP, and Their Analogs, Adjuvant Leads Against Latent HIV

Paul A. Wender,* Jung-Min Kee, Jeffrey M. Warrington

Although antiretroviral therapies have been effective in decreasing active viral loads in AIDS patients, the persistence of latent viral reservoirs prevents eradication of the virus. Prostratin and DPP (12-deoxyphorbol-13-phenylacetate) activate the latent virus and thus represent promising adjuvants for antiviral therapy. Their limited supply and the challenges of accessing related structures have, however, impeded therapeutic development and the search for clinically superior analogs. Here we report a practical synthesis of prostratin and DPP starting from phorbol or crotophorbolone, agents readily available from renewable sources, including a biodiesel candidate. This synthesis reliably supplies gram quantities of the therapeutically promising natural products, hitherto available only in low and variable amounts from natural sources, and opens access to a variety of new analogs.

AIDS is a pandemic disease caused by HIV. In a recent report, the Joint United Nations Programme on HIV/AIDS (UNAIDS) estimated that 33.2 million people were living with HIV and that 2.1 million people lost their lives to AIDS in the year 2007 (*1*).

Highly active antiretroviral therapy (HAART) has been successful in reducing HIV-1 levels in the plasma of many treated patients to undetectable levels. However, latent virus reservoirs remain in patients even after HAART (*2*). Such reservoirs are not targeted by current drug treatments, and as a consequence viral rebound often occurs if therapy is interrupted.

These latent viral reservoirs decrease only slowly in patients undergoing HAART. It is estimated that decades of treatment would be required to completely eliminate the latent virus. Such chronic treatment is undesirable because of the increased risk of side effects over time; the emergence of resistance through viral mutation; the increased demand on patients to maintain a long-term treatment regimen; and the cumulative financial burden of prolonged therapy, a particularly problematic issue in less-developed countries. Therefore, agents that can controllably flush the latent virus from its reservoirs could, in principle, provide a means to eradicate the virus when used as adjuvants in combination with HAART (*3*).

Although agents such as interleukin-2 and valproic acid have been tested as adjuvants in HAART, they cause toxicity or efficacy problems (*4*). Phorbol-13-myrisitate-12-acetate (PMA), a phorbol diester, is also reported to induce HIV-1 activation, but its potent tumor-promoting activity raises concerns about its therapeutic use (*5*, *6*).

Prostratin (**3**, 12-deoxyphorbol-13-acetate) and DPP (**4**, 12-deoxyphorbol-13-phenylacetate) are non–tumor-promoting 12-deoxytigliane diterpenes that exhibit potent in vitro activity in inducing HIV expression in latently infected cell lines and primary cells (*7*–*11*). Prostratin and DPP also inhibit HIV entry into target cells by down-regulating CD4 and CXCR4 receptors (*12*–*14*).

Department of Chemistry and Department of Chemical and Systems Biology, Stanford University, 337 Campus Drive, Stanford, CA 94305, USA.

*To whom correspondence should be addressed. E-mail: wenderp@stanford.edu

Downloaded from www.sciencemag.org on September 25, 2010